CELL BIOLOGY

A methylation-phosphorylation switch determines Plk1 kinase activity and function in DNA damage repair

Weizhe Li[1]*, Hong-Yan Wang[1]*, Xiaolu Zhao[1], Hongguo Duan[1], Binghua Cheng[2], Yafei Liu[1], Mengjie Zhao[1], Wenjie Shu[1], Yuchao Mei[1], Zengqi Wen[3], Mingliang Tang[1], Lin Guo[4], Guohong Li[3], Qiang Chen[2], Xiaoqi Liu[5,6], Hai-Ning Du[1]†

Polo-like kinase 1 (Plk1) is a crucial regulator of cell cycle progression; but the mechanism of regulation of Plk1 activity is not well understood. We present evidence that Plk1 activity is controlled by a balanced methylation and phosphorylation switch. The methyltransferase G9a monomethylates Plk1 at Lys209, which antagonizes phosphorylation of T210 to inhibit Plk1 activity. We found that the methyl-deficient Plk1 mutant K209A affects DNA replication, whereas the methyl-mimetic Plk1 mutant K209M prolongs metaphase-to-anaphase duration through the inability of sister chromatids separation. We detected accumulation of Plk1 K209me1 when cells were challenged with DNA damage stresses. Ablation of K209me1 delays the timely removal of RPA2 and RAD51 from DNA damage sites, indicating the critical role of K209me1 in guiding the machinery of DNA damage repair. Thus, our study highlights the importance of a methylation-phosphorylation switch of Plk1 in determining its kinase activity and functioning in DNA damage repair.

INTRODUCTION

Cell cycle progression is tightly controlled by many cell cycle regulators, including a series of kinases such as Cdk1, Plk1, and Aurora A (1, 2). It has been well documented that Plk1 participates in multiple transitions in mitosis, chromosome congression, sister chromatid separation, and cytokinesis (3–6). Mechanistically, Plk1 directly phosphorylates different substrates in a spatiotemporal-dependent manner, therefore regulating different cellular activities (1). Plk1 protein levels fluctuate during the cell cycle, in which the Plk1 levels peak in M phase and reach the lowest at early S phase (7). Plk1 kinase activity is tightly controlled during the entire cell cycle. At G$_2$ phase, Aurora A directly phosphorylates Plk1 on a conserved threonine residue (Thr^{210}) in the T-loop of the Plk1 kinase domain, with the synergistic action of Bora. Bora/Aurora A–dependent phosphorylation is required for full activation of Plk1 and for mitotic entry (8, 9). Elevated Plk1 levels and its activity have been found in many types of cancers and are correlated with poor prognosis (10, 11).

In addition to its crucial roles in mitotic events, accumulating evidence suggests that Plk1 is also involved in many nonmitotic events, such as DNA damage response (DDR) and G$_2$ DNA damage checkpoint recovery (9, 12). During the DDR process, the Mre11-Rad50-NBS1 (MRN) complex initially senses DNA breaks, promotes activation of protein kinases (ATM/ATR)–induced cascade, and enables the incorporation of RPA (replication protein A) proteins RPAs onto single-strand DNA (ssDNA). Subsequently, the mediator BRCA2-DSS1 complex aids the loading of the repair protein Rad51 onto RPA-bound ssDNA, triggers DNA pairing and strand invasion,

and eventually fixes DNA breaks (13). It has been reported that Plk1 activity can inactivate the ATR/Chk1 pathway through inhibiting 53BP1 targeting to DNA damage foci and degradation of the Chk1 activator Claspin (14, 15). In addition, Plk1-mediated MRe11 phosphorylation can also silence the DDR (16). Plk1 activity has to be blocked during the DDR by loss of threonine 210 phosphorylation (pT210) and dissociation of Aurora A, despite the fact that Plk1 activity is required for promoting checkpoint recovery and reactivation of the cell cycle machinery (9, 17). These observations suggest that intricate, yet precise regulation of Plk1 activity is executed during the DDR and checkpoint recovery. However, how Plk1 activity is switched on and off during this process is not fully understood.

Lysine methylation is predominantly catalyzed by a family of protein methyltransferases containing a catalytic SET [Su(var)3-9, Enhancer-of-zeste and Trithorax] (18). Methylation events at distinct lysine residues are linked to diverse functional outcomes. While lysine methylation on histones has been demonstrated to function in transcriptional regulation and epigenetic inheritance, abundant evidence supports lysine methylation on nonhistone proteins that can augment the signaling potentials of modified proteins and, as such, lead to various physiological consequences (19, 20). G9a, also known as EHMT2, has been shown to mono- or dimethylate a number of nonhistone proteins, including itself (21–23). For example, G9a methylates p53 and the myogenic regulator factor MyoD to inhibit their transactivation activity, whereas DNA ligase 1 methylated by G9a promotes the recruitment of UHRF1 and the maintenance of DNA methylation at DNA replication locus (24–26). It is noteworthy that a number of kinases are also substrates of methyltransferase. These methylation events could either enhance or inhibit the corresponding kinase activities, which have been shown to play roles in regulating proliferation, differentiation, and cell fate or repressing cancer (19).

In this study, we investigated the methylation of Plk1 by G9a and discovered that G9a efficiently monomethylates Plk1 at K209 residue. K209 methylation (K209me1) by G9a inhibits Plk1 kinase activity by antagonizing T210 phosphorylation (pT210) by Aurora

[1]Hubei Key Laboratory of Cell Homeostasis, College of Life Sciences, Wuhan University, Wuhan, Hubei 430072, China. [2]Medical Research Institute, School of Medicine, Wuhan University, Wuhan 430071, China. [3]National Laboratory of Biomacromolecules, CAS Center for Excellence in Biomacromolecules, Institute of Biophysics, Chinese Academy of Sciences ,Beijing 100101, China. [4]State Key Laboratory of Virology, College of Life Sciences, Wuhan University, Wuhan, Hubei 430072, China. [5]Department of Biochemistry, Purdue University, West Lafayette, IN, USA. [6]Center for Cancer Research, Purdue University, West Lafayette, IN, USA.
*These authors contributed equally to this work.
†Corresponding author. Email: hainingdu@whu.edu.cn

A. During the DDR, the interaction of G9a and Plk1 is enhanced, which promotes K209me1 and silences Plk1 kinase activity. By contrast, inhibition of DNA damage checkpoint activates Plk1 activity, at least in part, by removal of K209me1 marker. Hence, we present evidence that this methyl-phosphorylation switch coregulates Plk1 activity during the cell cycle and plays an important role in DNA damage repair.

## RESULTS

G9a can monomethylate Plk1

To examine whether Plk1 could be methylated, we immunoprecipitated Flag-tagged Plk1 that was stably expressed in HeLa S3 cells and examined the methylation status using an α-mono- and di-methyl lysine antibody. Western blot assays show that Plk1 could be methylated (Fig. 1A). To determine the modified sites, we subjected enriched Plk1 proteins to mass spectrometry analysis. Eventually, we identified a total of six monomethylated lysine sites but not di- or trimethylated lysine sites on Plk1, including K209, K284, K388, K420, K540, and K574 (fig. S1, A and B). Among these sites, the methylated K209 site particularly attracted our attention (Fig. 1B), as this site is in close proximity to T210, a critical site required for the full activation of Plk1 via Aurora A–mediated phosphorylation (8, 9). We speculate that these two types of modification on adjacent sites of Plk1 may have cross-talk and affect each other functionally. Another reason for our focus on K209me1 is that this methylated site is highly conserved among higher eukaryotic organisms (Fig. 1C). To confirm the occurrence of K209me1 in vivo, we generated a rabbit α-K209me1 polyclonal antibody. Dot blot analysis showed that this antibody specifically recognizes a synthetic K209me1 peptide but not a nonmethylated (K209me0) or a dimethylated K209 (K209me2) peptide (fig. S1C). Moreover, confirming its specificity, this antibody only recognized the methylated wild-type Plk1, either as the natural product enriched from cells (Fig. 1D, top) or as a synthetic peptide (Fig. 1D, bottom); it did not recognize either the K209R mutant or the recombinant Plk1 protein (Fig. 1D). To enhance the signal intensity of endogenous K209me1 recognized by this homemade antibody, we used HeLa S3 cells stably expressing Flag-tagged Plk1 in all the experiments described here unless specified otherwise. To avoid generating any artificial phenotype by expressing exogenous Plk1, we used a single clone that expresses Flag-Plk1 protein comparable to endogenous Plk1, and this clone also does not affect cell cycle progression and cellular localization of Plk1 (fig. S1D and see Fig. 4B).

Next, we sought to determine which methyltransferase is responsible for methylating Plk1 at the K209 site. To this end, several methyltransferases that have been reported to be capable to methylate nonhistone substrates were overexpressed in 293T cells, and the enzymes were immunoprecipitated using beads bearing proper epitopic tags (fig. S1E). We incubated the individual precipitate with the K209me0 peptide, and examined the reactants by dot blot analysis. The results indicate that only G9a, not other tested methyltransferases, can convert K209me0 to K209me1, as examined using the α-K209me1 antibody (Fig. 1E). To substantiate that G9a can directly methylate Plk1, we performed a series of experiments both in vitro and in vivo. First, immunoprecipitation assays indicated that G9a interacts with Plk1 and vice versa (fig. S1, F and G). Second, we performed in vitro methyltransferase assays using recombinant GST (glutathione S-transferase)–Plk1 incubated with bacterial purified G9a SET domain fragment. We measured total ^{3}H-acetyl incorporation by gel

and fluorography or by filter binding and liquid scintillation counting. It turns out that the G9a SET domain fragment, but not the MMSET SET domain fragment, demonstrates a robust activity on Plk1 in vitro (Fig. 1F). Consistently, enhanced green fluorescent protein (eGFP)–tagged full-length G9a purified from 293T cells, but not SET domain–defective G9a (ΔSET), can efficiently methylate the wild-type GST-tagged N-terminal Plk1 fragment, but not the K209R mutant (Fig. 1G). Third, consistent with our previous results, mass spectrometry analysis also identified monomethylation of K209 on Plk1 catalyzed by the recombinant G9a SET domain fragment in vitro, strengthening the notion of K209me1 on Plk1 modified by G9a (fig. S1H). Last, we observed that overexpression of G9a enhanced K209me1 levels, whereas knockdown of G9a by short hairpin RNA (shRNA) or knockout of G9a by CRISPR-Cas9 technique notably reduced K209me1 levels in cells (Fig. 1, H and I, and fig. S1, I and J). Together, these data suggest that G9a is the major, if not the sole, methyltransferase responsible for methylating K209 on Plk1.

Monomethylation of K209 by G9a and phosphorylation of T210 by Aurora A on Plk1 are mutually exclusive

It has been well documented that Aurora A–mediated T210 phosphorylation (pT210) of Plk1 is critical for Plk1 kinase activity (8, 9). Since K209 is adjacent to T210, could K209me1 by G9a affect pT210 by Aurora A and vice versa? Dot blot assays showed that Aurora A was only able to phosphorylate the K209me0 peptide, but not the K209me1 peptide (Fig. 2A). To rule out the possibility that the failure of detection of Aurora A–mediated phosphorylation on the K209me1 peptide is due to the inability of pT210 antibody recognition of the K209me1-containing peptide, we performed in vitro radioactive labeling analyses, in which the phosphorylation state of pT210 solely relies on incorporation of ^{32}P-labeled adenosine triphosphate (ATP) into the K209me1 peptide catalyzed by Aurora A. Despite the fact that the pT210 antibody we used here fails to recognize the K209me1/pT210 double-modified peptide, enriched Aurora A protein from cells can only phosphorylate the unmodified peptide, but not the methyl-modified peptide (Fig. 2B and fig. S2, A and B). These results suggest that K209me1 is likely to attenuate T210 phosphorylation by Aurora A. To further testify this conclusion, we performed in vitro methyltransferase assays using recombinant the N-Plk1 fragment incubated with or without G9a SET domain and then subsequently added with or without Aurora A protein (Fig. 2C). To avoid Plk1 autophosphorylation, we used the kinase-inactive version of Plk1 protein (K82M) in the sequential enzymatic reactions. We first confirmed that the enzyme-active G9a SET domain fragment was able to efficiently methylate the N-Plk1 fragment using liquid scintillation counting assays (Fig. 2D, top). Consistent with the results shown in the peptide assays, nonmethylated Plk1 protein exhibited robust radioactive phosphorylation by Aurora A compared to the methylated Plk1 protein measured by in vitro kinase assays (Fig. 2D, lane 3 versus lane 1, middle). Moreover, Western blot analysis showed that premethylated Plk1 at K209 by G9a attenuated pT210 of Plk1 by Aurora A (Fig. 2E). In addition, we also purified and used full-length Plk1 (bearing K82M kinase-inactive mutation) in the same sequential biochemical reactions described above. Although full-length Plk1 was methylated by G9a less efficiently than the N-Plk1 fragment, Aurora A exhibited more phosphorylation activity on the nonmethylated full-length Plk1 than on the methylated full-length Plk1 (fig. S3A). If we block Plk1 methylation on the K209 site by introduction of K209R mutation, Aurora A
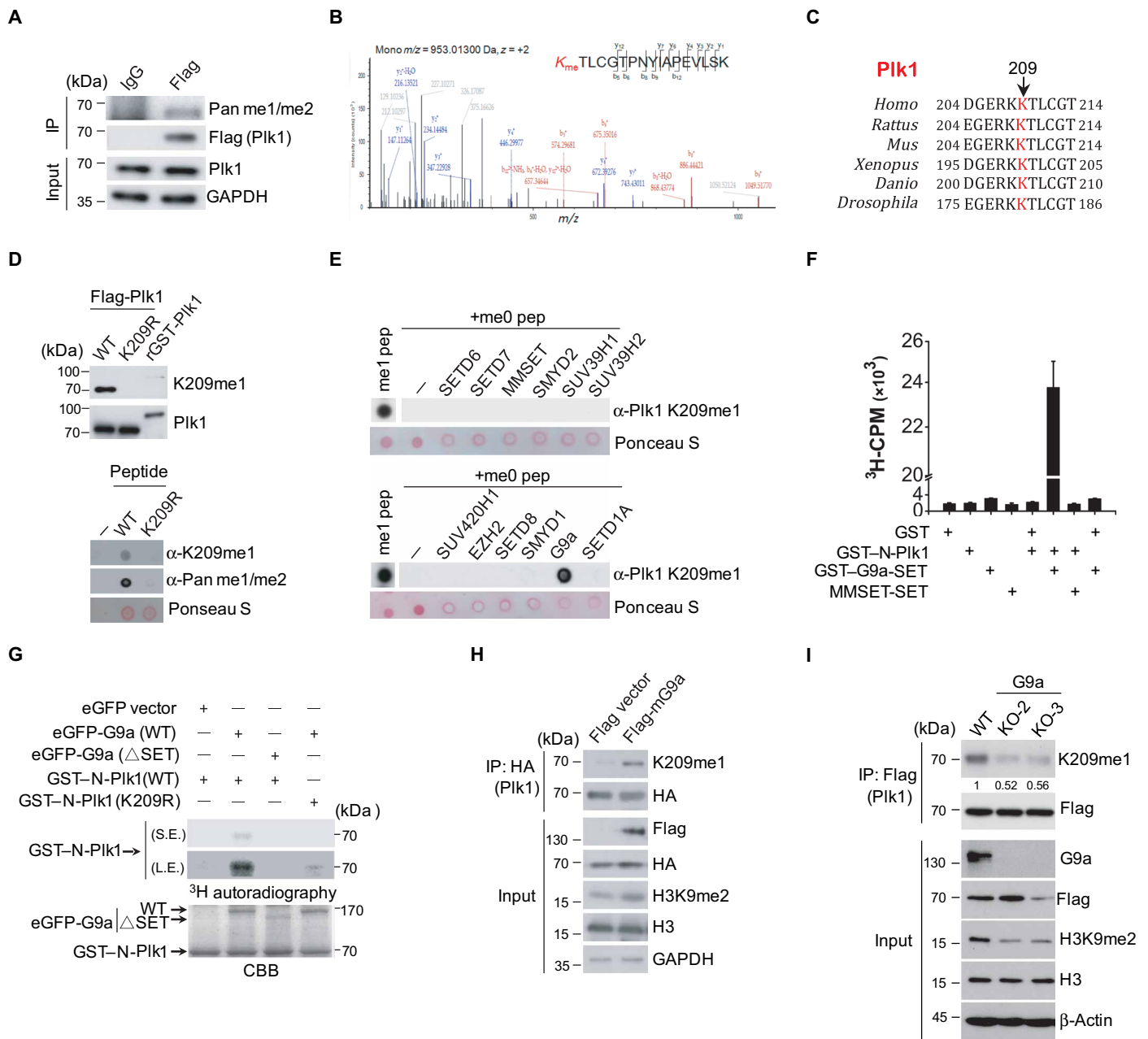
Fig. 1. Plk1 can be monomethylated on Lys209 by G9a. (**A**) Flag-tagged Plk1 was immunoprecipitated (IP) from HeLa S3 cells, and the methyl status of Plk1 was examined by probing with α-pan mono and dimethyl antibody (Pan me1/me2). IgG, immunoglobulin G. (**B**) Mass spectrum of Plk1 peptide shows K209 monomethylation. m/z, mass/charge ratio. (**C**) Alignment of the consensus Plk1 sequences between different species near the K209 methylation site. (**D**) Characterization of α-Plk1 K209me1-specific antibody. Top: Western blot analysis. Bottom: Dot blot analysis. (**E**) In vitro methylation assays were performed to examine enzymatic activities of various methyltransferases toward the nonmethylated K209 peptide (me0 pep) of Plk1 using the α-K209me1 antibody. A peptide bearing K209 monomethylation (me1 pep) served as a control. (**F**) In vitro methylation assays were performed and analyzed by liquid scintillation counting to measure ^{3}H incorporation using recombinant proteins. Three independent reactions with SDs are shown. CPM, count per minute. (**G**) In vitro methylation of the recombinant N-terminal fragment of Plk1 (GST–N-Plk1) by wild-type (WT) or SET domain–defective G9a (ΔSET). Top: Radioactive graph. Bottom: Coomassie brilliant blue staining (CBB). (**H** and **I**) Western blot analysis showing the effect of ectopically expressed mouse G9a (H) or knockout of G9a (I) on Plk1 K209me1. To increase K209me1 signal intensities, cells were synchronized at the G_1/S boundary in (I). S.E., short exposure; L.E., long exposure; GAPDH, glyceraldehyde phosphate dehydrogenase.

was still capable of more robustly phosphorylating the Plk1 K209R mutant than the "wild-type" Plk1 (fig. S3B). Furthermore, over-expression of G9a in HeLa S3 cells substantially decreased pT210 of Plk1 (Fig. 2F). The reduction of pT210 does not result from the

changes of cell cycle progression by overexpression of G9a, examined by fluorescence-activated cell sorting (FACS) analysis (fig. S3C). Cells treated with a specific inhibitor of G9a, BIX-01294, showed increased pT210 levels of Plk1 accompanied with a gradual decrease
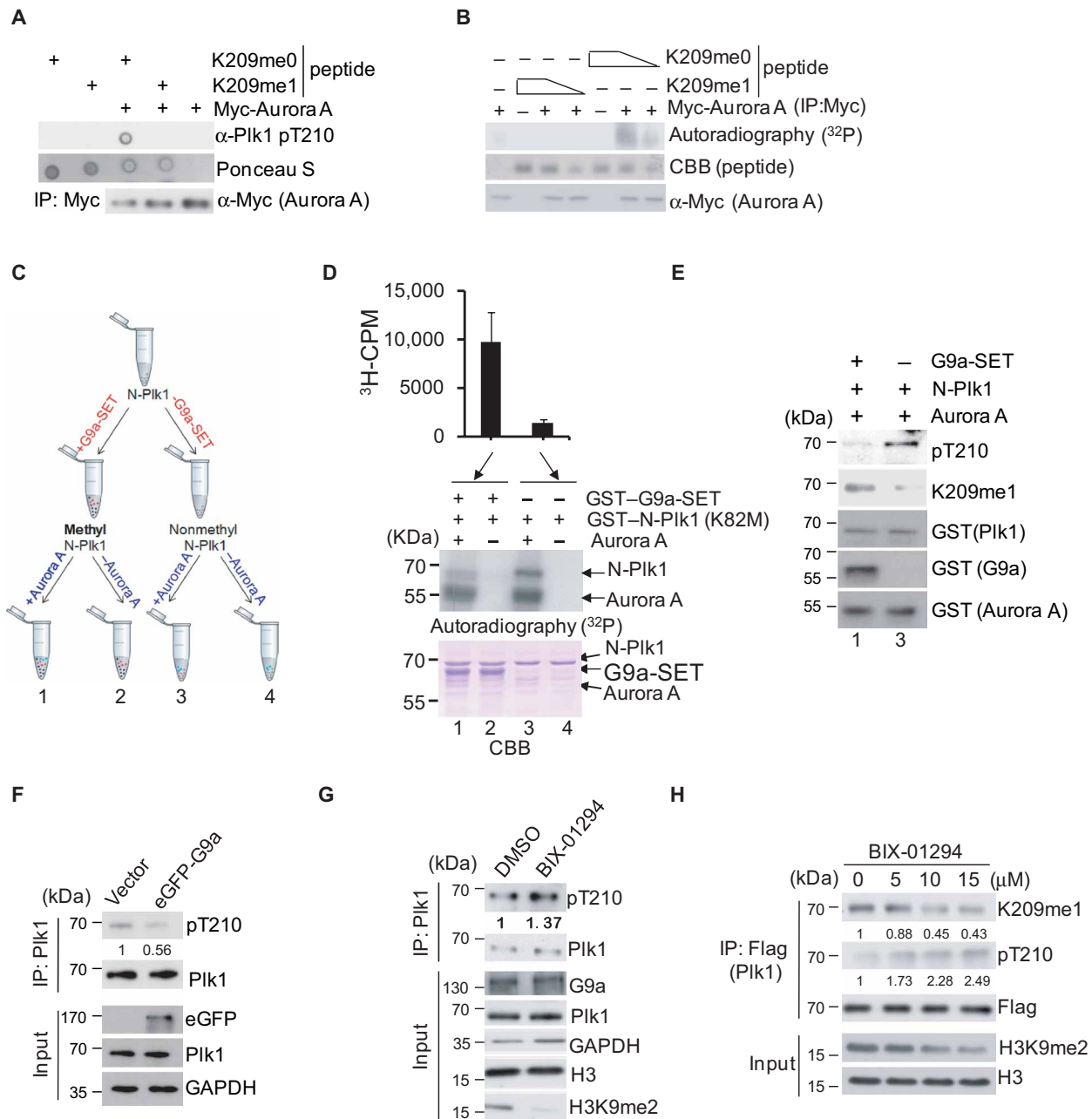
Fig. 2. K209me1 of Plk1 antagonizes pT210. (**A** and **B**) Dot blot analysis (A) or in vitro methylation assay (B) showing the kinase activity of Aurora A on different K209me methyl status of peptides. (**C** to **E**) After preincubated N-terminal fragment of Plk1 (N-Plk1 and K82M) with the SET domain fragment of G9a (G9a-SET), Aurora A–dependent Plk1 phosphorylation was examined. The numbers represent individual reactions. (C) Diagram of the sequential biochemical assays. (D) Liquid scintillation counting showing the methylation status of N-Plk1 by G9a (top); kinase assays showing the phosphorylation status of N-Plk1 by Aurora A (middle); the indicated proteins used in the sequential reactions were examined by Coomasie blue staining (bottom). The arrows represent the positions of purified recombinant proteins. (E) Western blot assay showing T210 phosphorylation (pT210) and K209 monomethylation (K209me1) status of Plk1 in the indicated reactions. (**F** to **H**) Western blot assay showing the effect of ectopically expressing G9a or G9a inhibitor BIX-01294 on Plk1 pT210 and K209me1 in HeLa S3 (F) or 293T (G and H) cells. The dose-dependent effects of BIX-01294 on the levels of K209me1 and pT210 of Plk1 are shown in (H). The H3K9me2 levels served as a control. The numbers below individual Western strips represent relative intensity of the corresponding band (pT210 or K209me1) normalized to the amount of immunoprecipitated Flag-Plk1 using ImageJ. DMSO, dimethyl sulfoxide.

in K209me1 levels in a dose-dependent manner (Fig. 2, G and H). Thus, these data demonstrate that K209me1 by G9a blocks pT210 of Plk1 by Aurora A.

To address whether T210 phosphorylation also inhibits K209 methylation, we also performed dot blot assays and liquid scintilla-

tion counting analysis. Consistently, we observed that G9a was only able to methylate the nonmethylated Plk1 peptide, but not with the pT210 moiety of Plk1 (Fig. 3, A and B). Furthermore, knockdown of Aurora A by expressing shRNA constructs in 293T cells remarkably increased K209me1 levels and accordingly decreased pT210

levels (Fig. 3C), whereas overexpression of Aurora A displayed opposite changes (Fig. 3D). These data support the notion that T210 phosphorylation by Aurora A, in turn, affects K209 monomethylation on Plk1.

### K209me1 of Plk1 peaks at S phase and may be required for DNA replication

To investigate the functional implications of Plk1 K209me1 catalyzed by G9a, we first determine the accumulation timing of K209me1 during the cell cycle. K209me1 reaches a higher level at the G_1/S boundary and drops at M phase, which is completely opposite to the status of pT210 (Fig. 4A, top). Notably, we revealed that Plk1 kinase activity appears to be inhibited by K209me1. As shown in the in vitro kinase assay using the same amount of substrate (casein in this case), Plk1 protein bearing abundant K209me1 modification exhibited much less kinase activity toward casein protein, compared to the similar quantitative amounts of Plk1 protein but bearing abundant pT210 moiety, suggesting the role of K209me1 in inhibiting Plk1 intrinsic activity (Fig. 4A, middle). To determine whether both K209me1 and pT210 levels are dynamically regulated during the entire cell cycle but in opposite directions, HeLa S3 cells stably ex-

pressing Flag-Plk1 were double thymidine–blocked and released into fresh medium. K209me1 levels in a series of cell samples taken at the different time points were examined by immunoprecipitation followed by Western blotting. As shown in Fig. 4B, K209me1 levels gradually declined from S phase to M phase, accompanied with an increase of pT210 levels, consistent with a previous observation that these two modifications on Plk1 per se exclude each other (Fig. 4B). Moreover, by doing coimmunoprecipitation assays, we found that the interactions between Plk1 and G9a or Aurora A are cell cycle dependent, as Plk1 mainly binds to G9a during S phase, whereas it binds to Aurora A during mitosis stage, suggesting distinct regulatory roles of these two modifications (Fig. 4C).

To investigate whether Plk1 K209me1 plays a role during S phase, we generated two HeLa/RFP-H2B cell lines with knock-in of a methyl-mimetic (K209M) or methyl-deficient (K209A) mutant using a CRISPR-Cas9 technique (fig. S4, A and B). We selected a single colony for each mutant, in which Plk1 expression levels are roughly equal and Plk1 localizations are identical to that of the wild-type cell line to ensure that any phenotype and consequences observed from the knock-in cell lines are not due to aberrant expression or mislocalization of endogenous Plk1 (fig. S4, C and D). HeLa/RFP-H2B cells
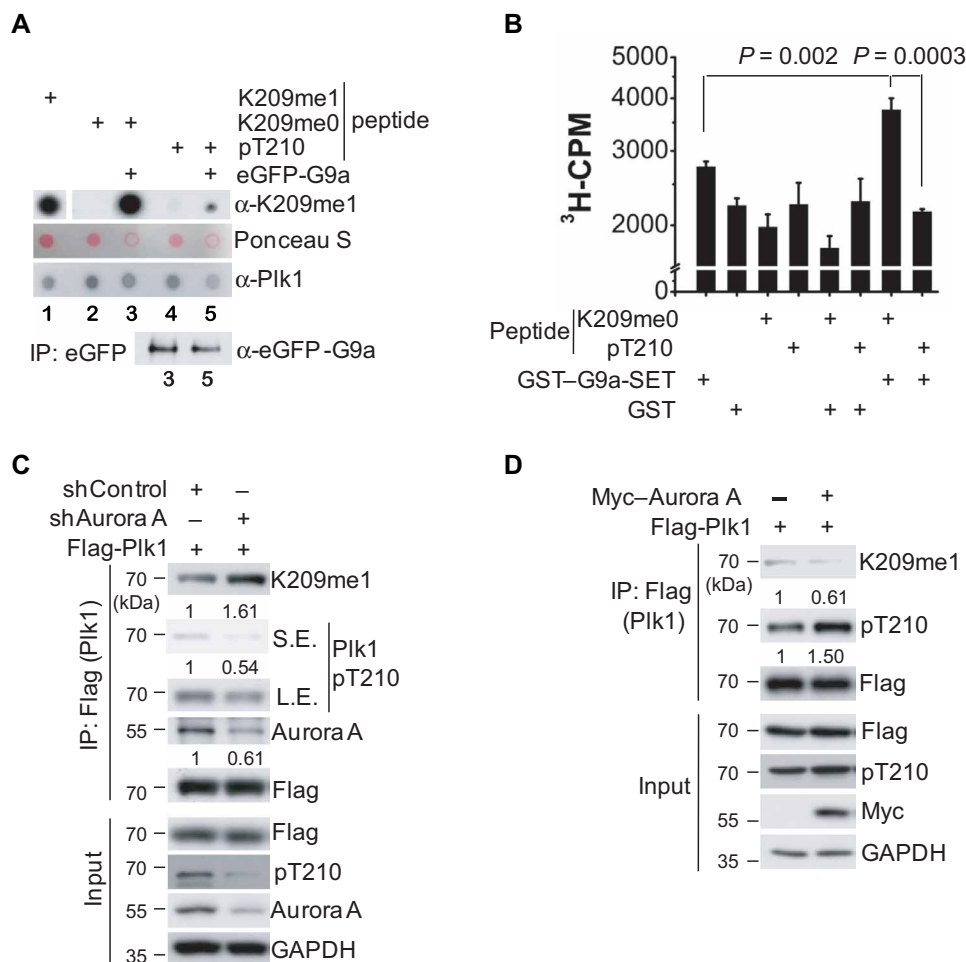
Fig. 3. Aurora A–mediated T210 phosphorylation blocks K209me1 of Plk1. (**A** and **B**) Dot blot analysis (A) or liquid scintillation counting (B) showing that G9a was able to methylate K209me0 peptide but barely able to methylate the phosphorylated T210 (pT210) and K209me1 peptides. (**C** and **D**) Western blot assay showing the effects of knockdown of Aurora A or ectopically expressing Aurora A on the K209me1 and pT210 levels of Plk1 in 293T cells. The numbers represent the relative intensity of corresponding band normalized to the amount of immunoprecipitated Flag-Plk1 using ImageJ.
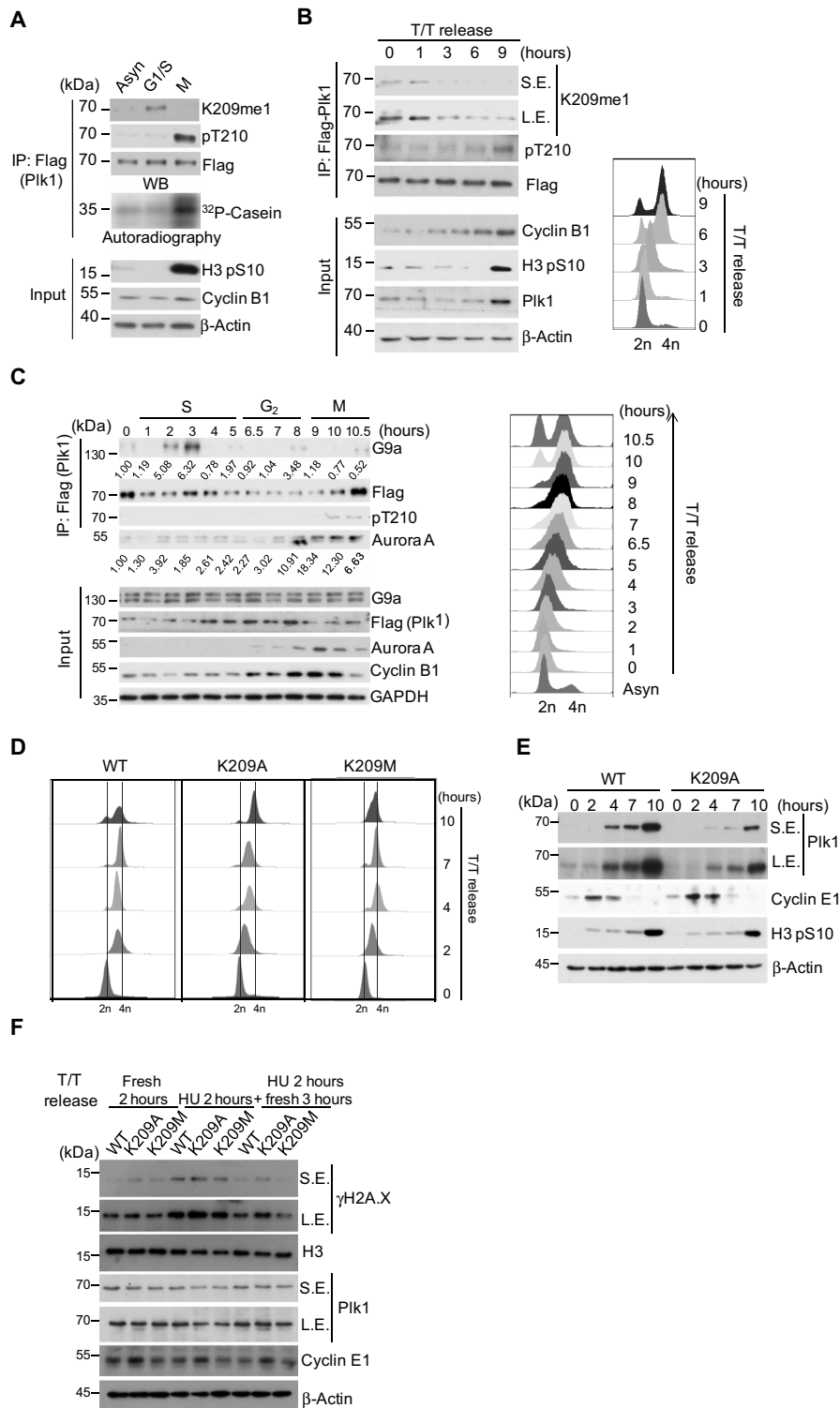
Fig. 4. Plk1 K209me1 peaks at S phase and the methylation attenuates its kinase activity. (**A**) Western blot analysis showing the antagonism of K209me1 and pT210 of Plk1 in synchronized G_1/S or mitotic cells. The immunoprecipitated Plk1 proteins were adjusted to similar levels. The kinase activity of immunoprecipitated Plk1 from the indicated cells on casein protein was measured by ^{32}P radioactive labeling assay. (**B**) Western blot assay showing the opposite changes of K209me1 and pT210 of stably expressed Flag-Plk1 in the double-thymidine (T/T) synchronized and released cells (left). The cell cycle profile was analyzed by FACS. (**C**) Western blot analysis showing the interactions of stably expressed Flag-Plk1 with G9a or Aurora A at different time points taken from the T/T-synchronized cells. Each number represents the relative binding intensities of G9a with Plk1 or the intensities of Aurora A with Plk1 (left). The cell cycle profile was analyzed by FACS (right). (**D** and **E**) The indicated cells taken from various time points after synchronized and released from T/T block were examined by FACS (D) or Western blot (E). (**F**) T/T-blocked cells were released into a different culture medium as indicated, and Western blot analyses were performed against the indicated antibodies. HU, hydroxyurea.

bearing the wild-type Plk1, K209A, or K209M mutant were synchronously released from a cell cycle arrest at the G_1/S boundary, and a series of cell samples were collected at the indicated time point. FACS analysis showed that K209A mutant, but not the wild-type Plk1 or K209M, significantly delayed S phase exit (Fig. 4D). This phenotype was confirmed by examining the dynamic levels of several cell cycle regulators using Western blot analysis (Fig. 4E). The degradation of cyclin E1 and the accumulation of Plk1were all retarded in K209A mutant cells compared to the wild-type, suggesting that K209me1 is required for S phase exit. Since DNA replication is the central event at S phase, we tested whether K209me1 plays a role in DNA replication. Three Plk1 cells were synchronized at the G_1/S boundary and released into fresh medium or medium containing the replication inhibitor hydroxyurea (HU) for 2 hours. As expected, three Plk1 cells displayed obvious replication stress upon exposure to HU treatment examined by immunblotting against γH2A.X, indicating occurrence of DNA damage checkpoint. After HU was washed off and cells continued growing for an additional 2 hours in fresh medium to allow cells to reenter the normal cell cycle, only K209A cells, but not the wild-type or K209M cells, still maintained substantial γH2A.X signals, suggesting the defect of K209A mutant to overcome DNA replication stress (Fig. 4F). The defect of K209A mutant probably does not rely on Plk1 activity, as the relative Plk1 activity of K209A mutant only shows a slight increase compared to those of the wild-type Plk1 or K209M mutant, which are enriched from synchronized S phase cells that stably express aforementioned Flag-Plk1 variants (fig. S4E). Although it is better to directly compare the kinase activities of those Plk1 variants by examining the phosphorylation status of T210, the pT210 antibody that we used here cannot recognize the K209A or K209M mutant (fig. S2C). Therefore, these results suggest that loss of Plk1 K209me1, instead of gain of Plk1 activity, may affect proper DNA replication.

Plk1 K209me1 severely delays metaphase-to-anaphase transition

Plk1 activation at G_2 phase is a prerequisite for mitotic entry (8). Since K209me1 levels gradually decline from G_1/S phase to M phase, we sought to determine the physiological requirement of K209me1 reduction at G_2 phase. Overexpression of the wild-type Plk1 in HeLa cells significantly increased mitotic index, determined by FACS with MPM2 staining or immunoblotting against the phosphorylated Ser[10] of histone H3 (pS10) (Fig. 5A). Notably, compared to the wild-type cells, the methyl-mimetic mutant K209M of Plk1 reduced mitotic cell population, whereas the methyl-defective mutant K209A significantly enhanced mitotic cell numbers (Fig. 5, A and B), which suggests that persistent K209me1 might affect mitotic entry and/or mitotic progression. To test this, HeLa/RFP-H2B cells bearing either wild-type Plk1 or K209M mutant were synchronously released from a cell cycle arrest at the G_1/S boundary (fig. S5). The Plk1 K209M mutant did not markedly delay G_2-to-M phase transition. However, the accumulation of histone H3 pS10 and the activation of Cdk1 (pY15) were slightly affected, indicating that the demethylation of K209me1 is required for G_2/M transition (fig. S5). Time-lapse analysis of mitotic progression upon visualization of RFP-H2B indicated that the duration from nuclear envelope breakdown to prometaphase was not altered, but the duration from metaphase to anaphase was significantly lengthened in K209M cells, but not in K209A cells (Fig. 5C and movies S1 to S3). We captured and examined ~20 cells from each cell line and found that, compared to the wild-

type cells, the duration of mitosis (from nuclear envelope breakdown to cytokenesis) was markedly increased from average 55 to 80 min in K209M cells, but not altered in K209A cells (Fig. 5D).

A prolonged metaphase may suggest a lack of tension across sister kinetochores (7, 27). Anaphase onset requires the establishment of interkinetochore tension, which is generated by the pulling force between kinetochore and microtubules. To examine whether the defects in K209M cells are due to a lack of tension, the interkinetochore distance was measured (7). The presence of the pulling force increased the interkinetochore distance in the wild-type cells from prometaphase (0.96 ± 0.14 µm) to metaphase (1.72 ± 0.22 µm). Unexpectedly, the interkinetochore distance in K209M or K209A cells was not altered either in prometaphase or in metaphase (fig. S6, A and B). In addition, the kinetochore signals of spindle checkpoint protein BubR1 at prometaphase or metaphase in K209M cells are comparable to those in the wild-type cells or K209A cells (fig. S6C). Thus, these results indicated that Plk1 methylation does not affect the kinetochore tension on the metaphase onset.

Alternatively, a prolonged metaphase may imply an impairment of sister chromatid separation. It has been shown that Plk1 activity is required for cohesin complex dissociation from chromosome arms (28). Is the lengthened duration from metaphase to anaphase in the Plk1 K209M cells related to the maintenance of arm cohesion? To answer this question, we treated cells with thymidine-nocodazole and harvested the late prometaphase cells shaken off from the arrested culture. We performed chromosome spreading and Giemsa staining to address whether arm cohesion is present (arms closed) or absent (arms open). As expected, arm cohesion was lost in ~80% of the nocodazole-treated cells (n > 150 cells, each bearing either wild-type or K209A Plk1). By contrast, more than 60% of the K209M cells still maintained arm cohesion after nocodazole treatment (Fig. 5, E and F, and fig. S6D). Moreover, we randomly chose 50 nocodazole-treated cells bearing either the wild-type or K209M mutant of Plk1, and we calculated the average interchromatid distance from five different sister chromatids of individual cells by measuring the distance at the farthest end of two sister chromatids from the centromere. Compared with the wild-type Plk1 cells, the interchromatid distance between two sister chromatids was significantly shortened by twofold in the K209M cells (Fig. 5G). Considering Plk1 activity is required for cohesin complex dissociation, we detected Plk1 activity from the wild-type Plk1 or K209A, K209M mutant using mitotic cells. By treating cells that stably express the aforementioned Flag-Plk1 variants with nocodazole, mitotic cells were shaken off, collected, and subjected to immunoprecipitation using α-Flag resins. We incubated the indicated Plk1 proteins with casein protein in the presence of radioactive-labeled ATP, and we performed in vitro phosphorylation assays. As shown in Fig. 5H, K209A mutant has much stronger activity toward casein, whereas K209M mutant has less activity, confirming its defective role in separation of sister chromatid. Together, these results conclude that the prolonged metaphase in the methyl-mimetic Plk1 cells mainly derived from the impairment of sister chromatid separation. The reduction of Plk1 K209me1 at mitosis is critical for cell cycle progression, especially for anaphase onset.

Plk1 K209me1 is not required for the activation of DNA damage checkpoint

Plk1 inactivation during G_2 phase in response to DNA damage is critical for preventing premature mitotic entry (9). But how Plk1 inactivation takes place during DNA damage is still obscure. Since
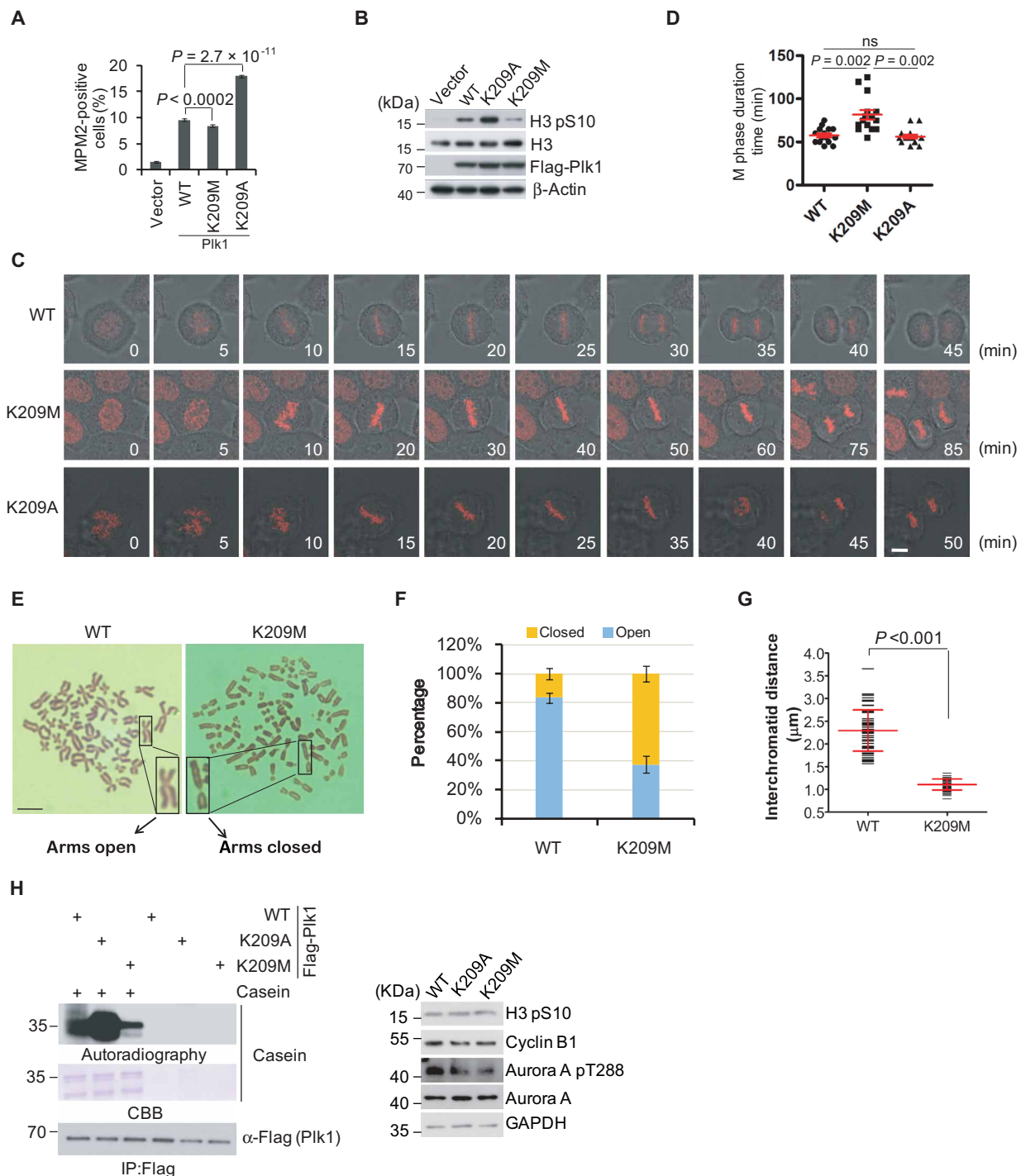
Fig. 5. Plk1 K209M mutant severely delayed metaphase-to-anaphase transition by preventing sister chromatid separation. (**A** and **B**) Mitotic cell populations in cells transfected with indicated Plk1 constructs were determined by FACS analysis staining with an α-MPM2 antibody, which specifically recognizes mitotic phosphoproteins (A), or using Western blot analysis (B). (**C** and **D**) Kinetics of mitotic progression in the indicated HeLa/RFP-H2B cells was analyzed by time-lapse microscopy. Cell images was captured every 5 min, and still frames from movies of representative cells are shown in (C). Scale bar, 10 μm. About 20 cell images from each cell line were captured, and the durations of mitotic progression were quantified in (D). (**E** to **G**) Arm cohesion of chromosomes in the wild-type or the K209M cells was analyzed by spreading and Giemsa staining. (E) Representative images from the indicated cells are shown, and insets show whether arm cohesion is absent (arm open) or present (arm closed). The ratio of open arms versus closed arms from more than 50 indicated cells each was quantified in (F). Scale bar, 100 μm. (G) The distance of sister chromatids at the arm ends from 50 indicated cells each was quantified. The error bars represent three independent experiments. (H) The mitotic cells stably expressing wild type, K209A, or K209M mutant of Flag-Plk1 were subjected to immunoprecipitation by α-Flag resins, the enriched Plk1 proteins were incubated with or without recombinant casein, and the Plk1 activities were measured by autoradiography (left). The mitotic cell cycle regulators were examined by immunoblotting (right). Data are presented as means ± SD in (A), (F), and (G). P values were determined by unpaired t test. ns, not significant.

herein we discovered that K209me1 of Plk1 by G9a counteracts with T210 phosphorylation by Aurora A, we speculated that K209me1 might play a role in cellular response to DNA damage. To this end, HeLa S3 cells were treated with the topoisomerase II inhibitor VP-16 (also called etoposide) or topoisomerase I inhibitor camptothecin (CPT) for 1 hour. Upon DNA damage reagent treatment, we observed an increase in K209me1 levels, accompanied with a reduction in pT210 levels, compared to the mock dimethyl sulfoxide (DMSO) treatment (Fig. 6A). Furthermore, HeLa S3 cells were released from a double-thymidine block for 6 hours to allow most cells entering G_2 phase, followed by the treatment with VP-16 or CPT. Consistently, we also observed an accumulation of K209me1 and the interaction of G9a with Plk1 under these stress conditions (Fig. 6B). Notably, the enhancement of K209me1 relies on the activation of DNA damage checkpoint, as inhibition of ATR by adding the ATR inhibitor VE-821 decreased the K209me1 levels and reactivated Plk1 T210 phosphorylation even in the presence of VP-16 or CPT (Fig. 6B). These results suggest that K209me1 is associated with DDR stress.

Given that an accumulation of γH2A.X has been widely used as a sensor of DNA lesion, we investigated whether K209me1 is required for the activation of DNA damage checkpoint by analyzing γH2A.X foci formation in the wild-type and K209A or K209M mutant cells using immunofluorescence staining. As shown in Fig. 6 (C and D), γH2A.X foci were exhibited in all the indicated cells 1 hour after DNA damage, but at 15 hours after VP-16 or CPT removal, the majority of γH2A.X foci returned to basal levels in wild-type or K209M cells, whereas K209A cells still exhibited visible γH2A.X foci (Fig. 6, C and D, and fig. S7, A and B). In addition, we observed that K209A cells failed to fix DNA resection 15 hours after the VP-16 or CPT removal examined by immunoblotting with phsophorylated Chk1 (Fig. 6E and fig. S7C). In agreement with our results, a previous study also showed that G9a knockout cells exhibited a prolonged staining of γH2A.X foci after removal of radiotherapeutic or chemotherapeutic treatment (29). Together, these results suggest that lack of K209 methylation is dispensable for the activation of DNA damage checkpoint but might impair downstream signaling cascade.

Plk1 K209me1 is unnecessary for the recruitment of DNA damage sensors to sites of DNA lesions

To explore how Plk1 methylation contributes to DDR cascade, we examined whether Plk1 may affect DNA damage–dependent recruitment of essential cellular factors that participate in the process. Therefore, we first examined whether the recruitment of Plk1 itself is deficient in Plk1 methyl-defective mutant. To this end, time-lapse imaging of micro-irradiated HeLa cells expressing GFP-tagged wild type, K209A, or K209M mutant of Plk1 was performed. Starting ~15 to 30 s after laser irradiation, all types of cells recruit Plk1 to sites of DNA damage in a similar pattern, confirming that Plk1 participates in DDR. However, Plk1 methylation seems not required for Plk1 recruitment to the DNA damage sites (fig. S8A). Next, we assessed the recruitment kinetics of HeLa cells bearing either the wild type or knock-in K209A/K209M mutants of Plk1 that transiently express GFP-tagged PARP1, NBS1, or RPA2 with live-cell imaging. PARP1 has been demonstrated to be the first wave of DNA damage sensors to mediate DNA damage repair factors to fix the lesions (30). As expected, PARP1 reached the DNA lesions in about 1 to 3 s after damage despite deficiency of Plk1 methylation (fig. S8B). Accordingly, the MRN complex subunit NBS1 was recruited after 10 to 15 s following

DNA damage, while the RPA2 accumulated at the DNA lesions in about 30 s following laser irradiation (fig. S8, C and D). However, there is no obvious difference in recruitment timing of those DNA damage repair factors between wild-type cells and K209A mutant cells, illustrating that Plk1 methylation is not required for recruitment of these factors to DNA damage sites that occurs at the early stage.

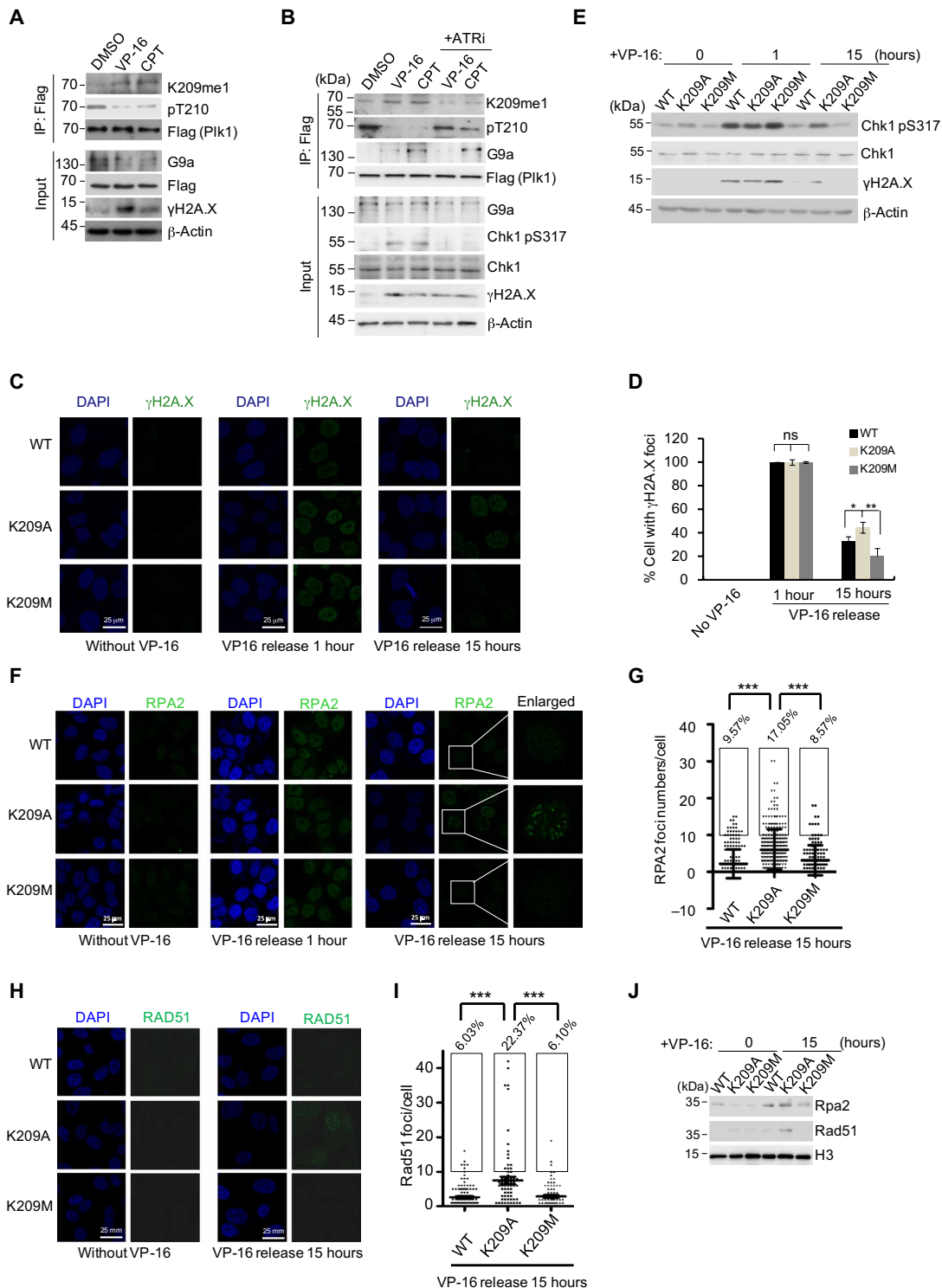### Plk1 K209me1 is required for DNA damage repair

The persistent activation of Chk1 in K209A cells after double-strand break (DSB) induction led us to ask whether this is due to a defect in DNA damage repair. By examining the accumulation and dissipation of RPA2 at DNA repair foci, we observed persistent retention of RPA2 in K209A cells compared to the wild-type cells or K209M mutant cells, indicating that K209 methylation contributes to DNA damage repair (Fig. 6, F and G, and fig. S7, D and E). Since RPA complex is required for chromatin loading of RAD51 and filament formation, we asked whether persistent RPA2 focus formation in methyl-deficient K209A cells was accompanied by an accumulation of RAD51 foci at the lesions. Even at 15 hours after VP-16 removal, we observed retention of RAD51 foci in the K209A cells but not in the wild-type or the K209M cells (Fig. 6, H and I). Moreover, compared with the wild-type Plk1 cells or the K209M cells, the methyl-deficient K209A cells exhibited a substantial increase in chromatin-bound RPA2 and RAD51 at 15 hours after VP-16 withdrawal, suggesting its inability of fixing DNA lesions (Fig. 6J). Together, these results suggest that DSB-induced Plk1 methylation may be required for the timely removal of RPA and RAD51 from DNA damage sites, which is essential for the completion of DNA damage repair.

DISCUSSION

Previous studies have demonstrated that Plk1 is activated in G_2 phase by the phosphorylation of T210 residue present in its T-loop before mitotic entry. The cooperation of two proteins, Bora and Aurora A, is crucial for this activation. Bora interacts with Plk1 in G_2 phase, which promotes Aurora A–catalyzed T210 phosporylation. These results, overall, unveil an activated regulatory mechanism toward Plk1 activity. In this study, we provided compelling evidence showing that a repressive regulation of Plk1 activity by lysine methylation inhibits the activation of Plk1 by competitively antagonizing phosphorylation on T210.

Once the methylation of Plk1 at K209 is validated, it is important to identify the methyltransferase involved. By screening a series of enzymes that have been reported to methylate nonhistone substrates, we revealed that only G9a, but not other tested methyltransferases, can efficiently methylate Plk1 K209 in vitro, indicating that Plk1 is a bona fide substrate of G9a (Fig. 1). Moreover, we also provided evidence that G9a is responsible for methylating the Lys209 site in vivo (Fig. 1H). Since several methylation sites of Plk1 were identified by mass spectrometry, other site-specific methyltransferases for Plk1 remain to be explored. Because knockout G9a in cells does not completely abolish K209me1, this raises the possibility that additional methyltransferases may play a minor role in methylating Plk1 at K209 (Fig. 1I).

It is intriguing that Plk1 methylation primarily occurs at S phase at which Plk1 expression is relatively low. Why does Plk1 have to be methylated during S phase? Several reports suggested that Plk1 may be unessential for unchallenged chromosomal DNA replication,

Fig. 6. Plk1 K209me1 is required for DNA damage repair. (**A**) Asynchronous cells stably expressing Flag-Plk1 were treated with VP-16 (40 μM) or CPT (2 μM) for 1 hour. Plk1 were immunoprecipitated using an α-Flag antibody, and samples were probed with the indicated antibodies. (**B**) Inhibition of ATR pathway by using the ATR inhibitor VE-821 (10 μM) resulted in premature mitotic entry. Synchronized G_2 cells were treated with VP-16 (40 μM) or CPT (2 μM) for 1 hour and an addition with or without VE-821 treatment for 2 hours. The changes of K209me1 and pT210 levels were examined by Western blot. (**C**, **F**, and **H**) The indicated cells were treated with VP-16 (40 μM for 1 hour) and allowed to release into normal medium for the indicated times and analyzed using immunofluorescent staining with an α-γH2A.X, α-RPA2, or α-RAD51 antibody, respectively. (**D**) Quantification of γH2A.X-positive cells in (C) using ImageJ. The data represent means ± SD (n > 100 each) from three independent experiments. (**E**) The indicated cells that were treated as described in (C) were analyzed using Western blotting. (**G** and **I**) Quantification of RPA2 or RAD51 foci numbers in individual cells described in (F) or (H) using ImageJ. The boxes designate cells with more than 10 foci, whose percentage is indicated above each box. ***$P < 0.001$. (**J**) The indicated cells were treated as described in (C), the chromatin fractions were collected, and chromatin-bound RPA2 and RAD51 levels were examined using Western blotting.

which is consistent with the observed phenotype of Plk1 inactivation in metazoan organisms (*31*). By contrast, under stress conditions, the DNA replication machinery frequently encounters damaged DNA templates that give rise to stalled replication by activating intra–S phase checkpoint. It has been demonstrated that Plk1 reactivation is required for bypassing stalled replication through the inactivation of the Chk1 pathway after prolonged cell cycle arrest (*15*, *32*). Thus, maintaining low activity of Plk1 at S phase likely favors timely triggering intra–S phase checkpoint during DNA replication, thereby maintaining genome integrity and preventing replication stress. Supporting this possibility, Lemmens *et al.* (*33*) recently reported that DNA replication during S phase restrains Plk1 and Cdk1 activities until S/G₂ transition. Suppression of DNA replication initiation led to prematurely activate Cdk1 and Plk1 and proceed to mitosis (*33*). Thus, on the basis of the observation of higher levels of K209me1 in S phase, we speculated that inactivation of Plk1 by K209 methylation is critical for preventing replication stress and premature mitotic entry. We also showed that G9a interacts with Plk1 more efficiently in S phase than in other cell cycle stages, and therefore, it is feasible that Plk1 is methylated at the highest levels during S phase. Note that the more detailed mechanism of how Plk1 K209me1 regulates DNA replication needs to be intensively explored.

Given that Plk1 is a key regulator of cell cycle progression, precise regulation of Plk1 activity becomes essential. We showed here that the activity of Plk1 is controlled by a balanced methylation and phosphorylation switch. The K209me1 levels gradually declined with cells released from S phase to M phase, accompanied with an enhancement of T210 phosphorylation. Despite our effort to explore the demethylase responsible for removal of the methyl mark on K209, we failed to identify any. However, we showed that methylation-mimetic mutant K209M severely prolonged mitotic progression, most likely due to its loss of the kinase activity, supporting the importance of Plk1 activation by demethylation of K209 and phosphorylation of T210 in the transition.

A very interesting finding in our study is the role of K209me1 in DDR (Fig. 6). During a DNA damage–induced arrest, phosphorylation of Plk1 on T210 has to be silenced by ATM activation on chromatin to prevent premature mitotic entry (*9*, *34*). Recently, Bruinsma *et al.* (*17*) proposed that the dissociation of Aurora A from the Plk1/Bora complex aids the inhibition of Plk1 activity. But how T210 dephosphorylation is established and why this dephosphorylation state is sustained in response to DNA damage are not known. Our study provides new clues to this event: Under DNA damage stress conditions, the interaction of G9a and Plk1 is enhanced, and K209 methylation on Plk1 is increased. Methylation of Plk1 is necessary neither for targeting itself to the DNA lesions nor for the recruitment of RPA and Rad51 to assemble the DNA repair machinery, but ablation of Plk1 methylation severely delays the timely removal of RPA complex and Rad51. A study from Inano *et al.* (*35*) suggests that an E3 ligase RFWD3 is critical for polyubiquitination and subsequent turnover of RPA and RAD51 at the DNA damage foci, which allows chromatin loading other DNA repair proteins to complete DNA repair progression. Therefore, it is likely that K209me1 provides a platform of some unknown DNA repair–related proteins, such as RFWD3, at the late stage to facilitate completion of DNA damage repair. Those observations illustrate the important role of K209me1 in silencing Plk1 activity and DNA damage repair, although further investigations are needed to understand how Plk1 methylation mediates the removal of DNA repair machinery. Of note, mounting evidence also points toward active roles of Plk1 in DDR, mainly by phosphorylation of a series of DNA damage–related proteins, including Rad51 and Claspin, to facilitate a homologous recombinant or adaptation of DNA checkpoint arrest (*36*–*38*). It is still unclear when and where the methylation-phosphorylation switch of Plk1 occurs, especially in the context of Plk1's role in DDR.

On the basis of our study, we propose a working model illustrating how a methyl-phosphorylation switch controls Plk1 activity and the critical roles of these two different modifications in DNA damage–induced cell cycle arrest or mitotic events, respectively. It is noteworthy that overexpression of Plk1 has been observed in a broad spectrum of cancers, and a series of small molecular inhibitors of Plk1 have been preclinically evaluated as potential drugs for cancer treatment (*11*). Given that G9a-mediated K209 methylation is able to inhibit Plk1 activity, our work might provide an alternative strategy through biological intervention of Plk1 activity for improving the efficacy of cancer therapy.

MATERIALS AND METHODS
Plasmids
Human full-length Plk1 was subcloned into a pCS2-3xFlag, pCS2-3xHA, pCDNA5.0-eGFP, or pGEX-6P-1 vector. Site-directed point mutations were generated using the QuikChange Site-Directed Mutagenesis protocol (Stratagene), and sequences were confirmed by DNA sequencing. The full-length Plk1 (K82M) and the N-Plk1 (1 to 371 amino acids, bearing K82M mutant) were subcloned into the pGEX-6P-1 vector. To screen the methyltransferases responsible for methylating Plk1, human full-length SETD6, SMYD1, SMYD2, SETD7, SUV39H1, SUV39H2, SUV420H1, and MMSET-SET were subcloned into the pCS2-3xFlag vector. Human full-length SETD8 and EZH2 were subcloned into the pCS2-3xHA vector. Human full-length Flag-SETD1A was obtained from M. Wu (Wuhan University). Human full-length eGFP-hG9a and mouse full-length Flag-mG9a were obtained from L. Zheng (Wuhan University). Human eGFP-hG9a-ΔSET (SET domain deleted), mouse Flag-mG9a-ΔSET (SET domain deleted), and Plk1 mutants were generated by site-directed mutagenesis. The SET domain of hG9a and MMSET were polymerase chain reaction (PCR)–amplified and subcloned into the pGEX-6P-1 vector. RPA2 was PCR-amplified and subcloned into the pEGFP-N3 vector. NBS1-GFP (pEGFP-N1 vector) was obtained from J. Huang (Zhejiang University). The SET domain of hG9a was also subcloned into pFastBac-GST for protein expression in insect cells. pCS2-3xMyc-AuroraA was described previously (*8*).

Antibodies and reagents
The following antibodies and reagents were obtained from commercial sources: The α-Plk1 (F-8) (sc-17783), α-HA (Y-11) (sc-805), and α-Wee1 (B-11) (sc-5285) antibodies were purchased from Santa Cruz Biotechnology; α-Flag (F7425-2MG) and α-Aurora A (A1231) antibodies were purchased from Sigma-Aldrich; α-G9a/EHMT2-(C6H3) (3306S) and α-pCdc2 (Y15) (4539T) antibodies were purchased from Cell Signaling Technology; α-cyclin B1 (1495-1), α-phospho histone H3 pS10 (1173-1), and α-phospho Plk1 pT210 (3646-1) antibodies were purchased from Epitomics; α-BubR1 (ab172581), α-RAD51 (ab133534), and α-H3K9me2 (ab1220) antibodies were purchased

from Abcam; α-eGFP (50430-2-AP), α-RPA2 (10412-1-AP), α-Myc (60003-2-Ig), and α-Actinβ (60008-1-Ig) antibodies were purchased from Proteintech; α-H3K9me2 (A2359) and mouse α-GAPDH (glyceraldehyde phosphate dehydrogenase) (AC002) antibodies were purchased from ABclonal; α-H3 (39163) antibody was purchased from Active Motif; pan-mono/dimethyl (TM602) antibody was purchased from PTM Biolabs; α-HEC1(9G3.23) (GTX70268) antibody was purchased from GeneTex; α-Plk1 K209me1 antibody was generated by ABclonal by immunizing rabbits with a K209-monomethylated peptide (DGERKK(me1)TLC) conjugated with keyhole limpet hemacyanin; secondary horseradish peroxidase–conjugated α-mouse or α-rabbit antibodies were purchased from Jackson ImmunoResearch Laboratories; the α-FLAG M2 affinity gel (A2220), thymidine, and nocodazole were purchased from Sigma-Aldrich; the α–hemagglutinin (HA) affinity gel (B23301) was purchased from BioTool; BIX-01294 was purchased from Selleck; VP-16 and VE-821 were purchased from TargetMol; and CPT was purchased from Aladin.

Cell culture, transfection, and treatment
The 293T, HeLa, and HeLa S3 cells and other stable cell lines were cultured in DMEM (Dulbecco's modified Eagle's medium) medium, supplemented with 10% fetal bovine serum, 2 mM L-glutamine, penicillin (100 U ml^{-1}), and streptomycin (100 μg ml^{-1}). The HeLa/RFP-H2B cell line was maintained in selective medium containing G418 (200 μg ml^{-1}). Cells were maintained at 37°C with 5% CO$_2$. Transfections were performed using Lipofectamine 2000 according to the manufacturer's instruction. Unless indicated, HeLa S3 cells were used in all of the cell experiments. For knockdown of Aurora A, the shRNA sequence was used: 5′-ACATACCAAGAGACCTA-CAA-3′. Cells were harvested between 36 and 48 hours after transfection and analyzed by immunoprecipitation and Western blotting. The G9a inhibitor BIX-01294 was added in different concentrations for 36 hours before harvest.

Cell synchronization
HeLa S3 cells were synchronized at the G$_1$/S boundary by a double-thymidine (T/T; 2 mM) treatment (18 hours of thymidine arrest and 8 hours of release, followed by 18 hours of thymidine arrest) and then released. Cells were synchronized at prometaphase by a thymidine-nocodazole (T/N) arrest [18 hours of thymidine arrest and 4 hours of release, followed by 12 hours of nocodazole arrest (100 ng ml^{-1})]. Mitotic cells were then collected by a shake-off method.

Coimmunoprecipitation and Western blotting
Cells were collected and lysed in immunoprecipitation (IP) buffer [25 mM tris-HCl (pH 7.4), 150 mM NaCl, 5% glycerol, 1 mM EDTA, and 1% NP-40] containing a protease inhibitor cocktail (BioTool) for 30 min on ice. The α-Flag resin or α-HA resin was added into the lysates and incubated at 4°C for 4 hours or overnight with rotation. After washed three times with IP buffer, the resins were resuspended into 2× SDS sample buffer, boiled, and centrifuged. Then, samples were subjected to SDS–polyacrylamide gel electrophoresis (SDS-PAGE), transferred to polyvinylidene difluoride membrane, and immunoblotted with the indicated antibodies.

Identification of Plk1 methylated sites by mass spectrometry
To identify in vivo methylation sites of Plk1, 293T cells were transfected with Flag-tagged Plk1. After 36 hours, the cells were harvested and lysated. Flag-Plk1 was immunoprecipitated by α-Flag resin and

subjected to SDS-PAGE. The band corresponding to Plk1 was subjected to in-gel trypsin digestion and desalted with C18 tips. The samples were analyzed by liquid chromatography–tandem mass spectrometry (LC-MS/MS) on a Q Exactive-HF mass spectrometer (Thermo Fisher Scientific). The LC-MS/MS data were processed using Proteome Discoverer (Thermo Fisher Scientific) and searched against the Swiss-prot Homo sapiens protein sequence database. The existence of monomethylation was verified on the basis of the occurrence of consecutive y or b ions and the mass increment of 14.016 Da on lysine residues.

In vitro methylation assays
For dot blot assays, 30 μg of aliquots of each of nonmethylated K209 peptide or phosphorylated T210 peptide of Plk1 was incubated with roughly 0.5 μg of methyltransferase moieties immunoprecipitated from 293T cells in the presence of 0.1 mM S-adenosyl-methionine (SAM; Sigma) at 30°C for 1 hour in the buffer [50 mM tris-HCl (pH 8.0), 10% glycerol, 20 mM KCl, 5 mM MgCl$_2$, and 1 mM phenylmethyl sulfonyl fluoride]. Reactions were spotted onto nitrocellulose membranes and immunoblotted with an α-Plk1 K209me1 antibody. The monomethylated Plk1 K209 peptide served as a control.

For protein methylation assays, 1-μg amount of bacterially or insect cell–expressed recombinant wild type or K209R GST–N-Plk1 was incubated overnight with G9a-SET fragments immunoprecipitated from 293T cells in the presence of 2 μCi of ^{3}H-labeled SAM at 30°C. Reactions were spotted onto P81 filters (Whatman) and washed four times with 50 mM NaHCO$_3$ (pH 9.0) before scintillation counting. Alternatively, reactions were quenched by adding an equal volume of 2× SDS sample buffer. Radiolabeled protein was separated by SDS-PAGE gel, followed by Coomassie blue staining or autoradiography.

In vitro kinase assays
Thirty micrograms of aliquots of each nonmethylated or monomethylated K209 peptide of Plk1 was incubated with Aurora A moiety immunoprecipitated from 293T cells at 30°C for 1 hour in the kinase reaction buffer [25 mM tris-HCl (pH 7.5), 0.01% Triton X-100, 10 mM MgCl$_2$, 0.5 mM Na$_3$VO$_4$, 2.5 mM dithiothreitol (DTT), and 0.5 mM EGTA] in the presence of 200 μM cold ATP or 1 μCi of γ-[^{32}P]ATP (PerkinElmer). Reactions were spotted onto a nitrocellulose membrane and immunoblotted against the indicated antibodies, or reactions were quenched with 2× SDS sample buffer and run in SDS-PAGE, followed by Coomassie staining or autoradiography.

Sequential in vitro methylation/phosphorylation assays
For Fig. 2C, 2 μg of recombinant GST-tagged N-Plk1 was incubated overnight with/without an equal amount of recombinant GST–G9a-SET at 30°C in the presence of 2 μCi of ^{3}H-labeled SAM. After that, a half volume of reaction mixture was examined by scintillation counting to verify the methylation of N-Plk1. The other half of mixture was added with 200 μM cold ATP and 0.5 μg of GST–Aurora A with buffer [25 mM tris-HCl, 10 mM MgCl$_2$, 2.5 mM DTT, 0.5 mM EGTA, and 0.1 μg μl^{-1} bovine serum albumin (BSA)] and reacted for an extra 1 hour. Reactions were stopped with 2× SDS sample buffer and examined by Coomassie staining or autoradiography.

Flow cytometry
Cells were harvested and washed in phosphate-buffered saline (PBS) before fixation in 70% ethanol in PBS at 4°C for 1 hour. Fixed cells

were washed once and resuspended in PBS containing 0.25% Triton X-100 and incubated on ice for 15 min. After centrifugation, the cell pellets were resuspended in 500 μl of PBS containing ribonuclease A (10 μg ml^{-1}; Sigma) and propidium iodide (20 μg ml^{-1}; Sigma), transferred to FACS tubes, and incubated at room temperature in the dark for 30 min. Cell cycle analysis was performed using Summit 3.0 software. A minimum of 1×10^4 events were collected for each sample, and all conditions were performed in triplicate.

Immunofluorescent staining
Cells were cultured on glass coverslips, fixed with 4% paraformaldehyde for 10 min at room temperature, and permeabilized with 0.3% Triton X-100 for 30 min. Then, cells were blocked with 3% BSA in PBS and incubated overnight for 30 min at room temperature or 4°C. Then, cells were incubated overnight with the indicated primary antibody for 2 hours at room temperature or 4°C. After washed with PBS three times, cells were incubated for 1 hour at room temperature with the appropriate secondary antibody. The coverslips were stained with 4′,6-diamidino-2-phenylindole and mounted. Immunofluorescence images were captured under a confocal laser scanning microscope (Leica SP8).

Time-lapse imaging and laser micro-irradiation
HeLa/RFP-H2B stable cell lines were seeded in an eight-chambered cover glass (Lab-Tek Chambered Borosilicate Coverglass System, Nunc). Cells were synchronized by T/T block and release following the procedure described above. Cells were placed in a 37°C-heated microscope chamber and observed under an inverted fluorescence microscope (Leica SP8) with a 63× lens. Images were acquired in the 561 channel every 5 min and captured for a total of 5 hours. Images were viewed and analyzed using Leica LAS AF Lite software. Laser micro-irradiation was performed as described previously (*39*). Briefly, cell cultured on glass-bottomed 35-mm dishes were micro-irradiated using a computer-controlled MicroPoint laser Ablation System (365 nm; Andor Company) coupled with an Olympus IX83 inverted microscope (60× oil-immersion objective). Time-lapse images of live cells were taken under the same microscope with the MetaMorph Microscope Automation & Image Analysis software.

Protein expression and purification
BL21(DE3) plysS–competent cells bearing plasmids encoding GST, GST–N-Plk1, or GST–MMSET-SET were induced with 0.2 mM isopropyl-β-ᴅ-thiogalactopyranoside (IPTG) at 30°C for 4 hours. BL21(DE3) pTf16–competent cells bearing a plasmid encoding GST–G9a-SET was induced with 0.1 mM IPTG and ʟ-arabinose (0.5 mg ml^{-1}) at 16°C for 8 hours.

For protein expression and purification in Sf9 insect cells, G9a-SET construct was subcloned into a pFastBac-GST plasmid. Recombinant baculoviruses were generated according to the manufacturer's protocol (Invitrogen). When expressing proteins at large scale, the Sf9 cells were grown in an orbital shaker at 27°C at a constant stirring rate of 100 rpm in the dark. The baculoviruses were added to the Sf9 cells at a density of 1×10^6 cells ml^{-1}, and the cells were harvested around 72 hours after transduction. Cells were lysed in buffer containing 50 mM tris-HCl, 150 mM NaCl, and 0.05% NP-40, and proteins were purified using a glutathione-Sepharose resin (Aogma), followed by elution with glutathione [20 mM in 75 mM tris-HCl (pH 8.0)] and dialysis.

Generation of knockout or knock-in cell lines
For CRISPR-Cas9 genome editing, a plasmid encoding both the Cas9 protein and the guide RNA (gRNA) was used. pSpCas9(BB)-2A-Puro(pX459) V2.0 from Addgene (plasmid no. 62988) was used for G9a knockout. pX260 remolded by G.L.'s laboratory was used for Plk1 knock-in. gRNA targets with high activity and specificity were designed with the online software from Z. Feng's laboratory (http://crispr.mit.edu/) and inserted into the gRNA cloning vector. G9a-sgRNA-2, CACC GTCTCGGAAACGGCGCAAGC; G9a-sgRNA-3, CACCGATTGACCGCATCAGCGAGA. For Plk1 K209M/A knock-in, we used pMD19 as the donor vector. About 1 kb of Plk1 genome sequence around lysine 209 (500 bp of the upper part and 500 bp of the lower part served as homology arms) was inserted into pMD19, followed by point mutation K209M/A using the QuikChange Site-Directed Mutagenesis protocol.

Single-cell colony screening and validation
pX459-G9a-sgRNAs were transfected into HeLa S3 cells. pX260-Plk1-sgRNA and pMD19-Plk1-K209M/A were transfected into HeLa/RFP-H2B cells. Then, the edited cells were selected by adding puromycin (1 μg ml^{-1}). The positive clones were collected and plated onto 96-well plates at a concentration of approximately one cell per well. One week later, the single-colony cells were selected for validation using a combination of Western blot assay and genomic sequencing.

Giemsa staining
HeLa/RFP-H2B cell lines bearing the K209A or K209M mutant were synchronized by T/N block and release as described above. Harvested cells were treated with 0.075 M KCl hypotonic buffer at a 37°C water bath for 15 min, followed by fixation with methanol:acetic acid (3:1, v/v). Cell suspensions were dropped onto cleaned slides and air-dried. The slides were stained with a diluted Giemsa solution for 10 min and then were washed by water and air-dried. Images were acquired by Leica DM1000 and analyzed using Leica Application Suite V3 software.

Chromatin fractionation
Preparation of chromatin fractions was as described previously with minor modifications (*40*). Briefly, 1 hour after treatment with VP-16, cells were washed three times with PBS and maintained with fresh medium without VP-16 for 15 hours. Cells were then collected, and cell pellets were subsequently resuspended in buffer [20 mM tris-HCl, (pH 8.0), 100 mM NaCl, 1 mM EDTA, and 0.5% NP-40] and incubated on ice for 20 min. Nuclei were then collected and resuspended in HCl (0.2 M). The soluble fraction was neutralized with tris-HCl (1 M at pH 8.0) for further analysis.

Quantification and statistical analysis
For quantification of the Western blot data, ImageJ software was used to measure the relative intensity of each band, and the relative protein or modification levels were normalized to the relative loading control levels. Unless otherwise indicated, data are presented as the means ± SD from at least three independent experiments, and the differences between any two groups were compared by unpaired *t* tests. The data were scatter-plotted using the Prism 5 software. $*P < 0.05$, $**P < 0.01$, $***P < 0.001$, and ns indicates "not significant."

SUPPLEMENTARY MATERIALS

Supplementary material for this article is available at http://advances.sciencemag.org/cgi/content/full/5/3/eaau7566/DC1

Fig. S1. Identification of the methyltransferase responsible for methylating Plk1.

Fig. S2. Validation of K209me1 or pT210 antibody recognition of various peptides and mutant cells.

Fig. S3. K209me1 of Plk1 antagonizes pT210.

Fig. S4. Generation of K209A and K209M knock-in Plk1 mutant cell lines.

Fig. S5. Plk1 K209M mutant slightly delays G_2/M transition.

Fig. S6. Plk1 K209me1 does not affect the kinetochore tension on the metaphase onset.

Fig. S7. Plk1 K209me1 is required for DNA damage repair.

Fig. S8. Plk1 K209me1 is not required for the recruitment of DNA damage factors to DNA damage sites.

Movie S1. A representative HeLa/RFP-H2B cell bearing wild-type Plk1 was recorded from nuclear breakdown to cytokinesis by time-lapse microscopy.

Movie S2. A representative HeLa/RFP-H2B cell bearing K209A mutant Plk1 was recorded from nuclear breakdown to cytokinesis by time-lapse microscopy.

Movie S3. A representative HeLa/RFP-H2B cell bearing K209M mutant Plk1 was recorded from nuclear breakdown to cytokinesis by time-lapse microscopy.

Movie S4. A population of HeLa/RFP-H2B cells bearing K209M mutant Plk1 was recorded from nuclear breakdown to cytokinesis by time-lapse microscopy.

REFERENCES AND NOTES

1. T. Takaki, K. Trenz, V. Costanzo, M. Petronczki, Polo-like kinase 1 reaches beyond mitosis—Cytokinesis, DNA damage response, and development. *Curr. Opin. Cell Biol.* **20**, 650–660 (2008).

2. H. Hochegger, S. Takeda, T. Hunt, Cyclin-dependent kinases and cell-cycle transitions: Does one fit all? *Nat. Rev. Mol. Cell Biol.* **9**, 910–916 (2008).

3. W. Bruinsma, J. A. Raaijmakers, R. H. Medema, Switching Polo-like kinase-1 on and off in time and space. *Trends Biochem. Sci.* **37**, 534–542 (2012).

4. C. R. Paschal, J. Maciejowski, P. V. Jallepalli, A stringent requirement for Plk1 T210 phosphorylation during K-fiber assembly and chromosome congression. *Chromosoma* **121**, 565–572 (2012).

5. M. Petronczki, P. Lénárt, J.-M. Peters, Polo on the rise—From mitotic entry to cytokinesis with Plk1. *Dev. Cell* **14**, 646–659 (2008).

6. X. Wang, Y. Yang, Q. Duan, N. Jiang, Y. Huang, Z. Darzynkiewicz, W. Dai, sSgo1, a major splice variant of Sgo1, functions in centriole cohesion where it is regulated by Plk1. *Dev. Cell* **14**, 331–341 (2008).

7. A. Seki, J. A. Coppinger, H. Du, C.-Y. Jang, J. R. Yates III, G. Fang, Plk1- and β-TrCP–dependent degradation of Bora controls mitotic progression. *J. Cell Biol.* **181**, 65–78 (2008).

8. A. Seki, J. A. Coppinger, C.-Y. Jang, J. R. Yates III, G. Fang, Bora and the kinase Aurora a cooperatively activate the kinase Plk1 and control mitotic entry. *Science* **320**, 1655–1658 (2008).

9. L. Macůrek, A. Lindqvist, D. Lim, M. A. Lampson, R. Klompmaker, R. Freire, C. Clouin, S. S. Taylor, M. B. Yaffe, R. H. Medema, Polo-like kinase-1 is activated by aurora A to promote checkpoint recovery. *Nature* **455**, 119–123 (2008).

10. K. Strebhardt, A. Ullrich, Targeting polo-like kinase 1 for cancer therapy. *Nat. Rev. Cancer* **6**, 321–330 (2006).

11. R. E. Gutteridge, M. A. Ndiaye, X. Liu, N. Ahmad, Plk1 inhibitors in cancer therapy: From laboratory to clinics. *Mol. Cancer Ther.* **15**, 1427–1435 (2016).

12. V. A. J. Smits, R. Klompmaker, L. Arnaud, G. Rijksen, E. A. Nigg, R. H. Medema, Polo-like kinase-1 is a target of the DNA damage checkpoint. *Nat. Cell Biol.* **2**, 672–676 (2000).

13. M. S. Y. Huen, J. Chen, Assembly of checkpoint and repair machineries at DNA damage sites. *Trends Biochem. Sci.* **35**, 101–108 (2010).

14. M. A. T. M. van Vugt, A. K. Gardino, R. Linding, G. J. Ostheimer, H. C. Reinhardt, S.-E. Ong, C. S. Tan, H. Miao, S. M. Keezer, J. Li, T. Pawson, T. A. Lewis, S. A. Carr, S. J. Smerdon, T. R. Brummelkamp, M. B. Yaffe, A mitotic phosphorylation feedback network connects Cdk1, Plk1, 53BP1, and Chk2 to inactivate the G_2/M DNA damage checkpoint. *PLOS Biol.* **8**, e1000287 (2010).

15. I. Mamely, M. A. T. M. van Vugt, V. A. J. Smits, J. I. Semple, B. Lemmens, A. Perrakis, R. H. Medema, R. Freire, Polo-like kinase-1 controls proteasome-dependent degradation of Claspin during checkpoint recovery. *Curr. Biol.* **16**, 1950–1955 (2006).

16. Z. Li, J. Li, Y. Kong, S. Yan, N. Ahmad, X. Liu, Plk1 phosphorylation of Mre11 antagonizes the DNA damage response. *Cancer Res.* **77**, 3169–3180 (2017).

17. W. Bruinsma, M. Aprelia, I. García-Santisteban, J. Kool, Y. J. Xu, R. H. Medema, Inhibition of Polo-like kinase 1 during the DNA damage response is mediated through loss of Aurora A recruitment by Bora. *Oncogene* **36**, 1840–1848 (2017).

18. H.-M. Herz, A. Garruss, A. Shilatifard, SET for life: Biochemical activities and biological functions of SET domain-containing proteins. *Trends Biochem. Sci.* **38**, 621–639 (2013).

19. K. K. Biggar, S. S.-C. Li, Non-histone protein methylation as a regulator of cellular signalling and function. *Nat. Rev. Mol. Cell Biol.* **16**, 5–17 (2015).

20. C. Martin, Y. Zhang, The diverse functions of histone lysine methylation. *Nat. Rev. Mol. Cell Biol.* **6**, 838–849 (2005).

21. M. Tachibana, K. Sugimoto, T. Fukushima, Y. Shinkai, Set domain-containing protein, G9a, is a novel lysine-preferring mammalian histone methyltransferase with hyperactivity and specific selectivity to lysines 9 and 27 of histone H3. *J. Biol. Chem.* **276**, 25309–25317 (2001).

22. X. Zhang, D. Peng, Y. Xi, C. Yuan, C. A. Sagum, B. J. Klein, K. Tanaka, H. Wen, T. G. Kutateladze, W. Li, M. T. Bedford, X. Shi, G9a-mediated methylation of ERα links the PHF20/MOF histone acetyltransferase complex to hormonal gene expression. *Nat. Commun.* **7**, 10810 (2016).

23. L. Bao, Y. Chen, H.-T. Lai, S.-Y. Wu, J. E. Wang, K. J. Hatanpaa, J. M. Raisanen, M. Fontenot, B. Lega, C.-M. Chiang, G. L. Semenza, Y. Wang, W. Luo, Methylation of hypoxia-inducible factor (HIF)-1α by G9a/GLP inhibits HIF-1 transcriptional activity and cell migration. *Nucleic Acids Res.* **46**, 6576–6591 (2018).

24. J. Huang, J. Dorsey, S. Chuikov, X. Zhang, T. Jenuwein, D. Reinberg, S. L. Berger, G9a and Glp methylate lysine 373 in the tumor suppressor p53. *J. Biol. Chem.* **285**, 9636–9641 (2010).

25. B. M. T. Ling, N. Bharathy, T.-K. Chung, W. K. Kok, S. Li, Y. H. Tan, V. K. Rao, S. Gopinadhan, V. Sartorelli, M. J. Walsh, R. Taneja, Lysine methyltransferase G9a methylates the transcription factor MyoD and regulates skeletal muscle differentiation. *Proc. Natl. Acad. Sci. U.S.A.* **109**, 841–846 (2012).

26. L. Ferry, A. Fournier, T. Tsusaka, G. Adelmant, T. Shimazu, S. Matano, O. Kirsh, R. Amouroux, N. Dohmae, T. Suzuki, G. J. Filion, W. Deng, M. de Dieuleveult, L. Fritsch, S. Kudithipudi, A. Jeltsch, H. Leonhardt, P. Hajkova, J. A. Marto, K. Arita, Y. Shinkai, P.-A. Defossez, Methylation of DNA ligase 1 by G9a/GLP recruits UHRF1 to replicating DNA and regulates DNA methylation. *Mol. Cell* **67**, 550–565.e5 (2017).

27. H. Maiato, J. DeLuca, E. D. Salmon, W. C. Earnshaw, The dynamic kinetochore-microtubule interface. *J. Cell Sci.* **117**, 5461–5477 (2004).

28. J. F. Giménez-Abián, I. Sumara, T. Hirota, S. Hauf, D. Gerlich, C. de la Torre, J. Ellenberg, J.-M. Peters, Regulation of sister chromatid cohesion between chromosome arms. *Curr. Biol.* **14**, 1187–1193 (2004).

29. Q. Yang, Q. Zhu, X. Lu, Y. Du, L. Cao, C. Shen, T. Hou, M. Li, Z. Li, C. Liu, D. Wu, X. Xu, L. Wang, H. Wang, Y. Zhao, Y. Yang, W.-G. Zhu, G9a coordinates with the RPA complex to promote DNA damage repair and cell survival. *Proc. Natl. Acad. Sci. U.S.A.* **114**, E6054–E6063 (2017).

30. C. Liu, A. Vyas, M. A. Kassab, A. K. Singh, X. Yu, The role of poly ADP-ribosylation in the first wave of DNA damage response. *Nucleic Acids Res.* **45**, 8129–8141 (2017).

31. K. Trenz, A. Errico, V. Costanzo, Plx1 is required for chromosomal DNA replication under stressful conditions. *EMBO J.* **27**, 876–885 (2008).

32. M. A. T. M. van Vugt, A. Brás, R. H. Medema, Polo-like kinase-1 controls recovery from a G2 DNA damage-induced arrest in mammalian cells. *Mol. Cell* **15**, 799–811 (2004).

33. B. Lemmens, N. Hegarat, K. Akopyan, J. Sala-Gaston, J. Bartek, H. Hochegger, A. Lindqvist, DNA replication determines timing of mitosis by restricting CDK1 and PLK1 activation. *Mol. Cell* **71**, 117–128.e3 (2018).

34. H. Jaiswal, H. Benada, E. Müllers, K. Akopyan, K. Burdova, T. Koolmeister, T. Helleday, R. H. Medema, L. Macurek, A. Lindqvist, ATM/Wip1 activities at chromatin control Plk1 re-activation to determine G2 checkpoint duration. *EMBO J.* **36**, 2161–2176 (2017).

35. S. Inano, K. Sato, Y. Katsuki, W. Kobayashi, H. Tanaka, K. Nakajima, S. Nakada, H. Miyoshi, K. Knies, A. Takaori-Kondo, D. Schindler, M. Ishiai, H. Kurumizaka, M. Takata, RFWD3-mediated ubiquitination promotes timely removal of both RPA and RAD51 from DNA damage sites to facilitate homologous recombination. *Mol. Cell* **66**, 622–634.e8 (2017).

36. H. Y. Yoo, A. Kumagai, A. Shevchenko, A. Shevchenko, W. G. Dunphy, Adaptation of a DNA replication checkpoint response depends upon inactivation of Claspin by the Polo-like kinase. *Cell* **117**, 575–588 (2004).

37. R. G. Syljuasen, S. Jensen, J. Bartek, J. Lukas, Adaptation to the ionizing radiation–induced G_2 checkpoint occurs in human cells and depends on checkpoint kinase 1 and Polo-like kinase 1 kinases. *Cancer Res.* **66**, 10253–10257 (2006).

38. K. Yata, J. Lloyd, S. Maslen, J.-Y. Bleuyard, M. Skehel, S. J. Smerdon, F. Esashi, Plk1 and CK2 act in concert to regulate Rad51 during DNA double strand break repair. *Mol. Cell* **45**, 371–383 (2012).

39. J. Lou, H. Chen, J. Han, H. He, M. S. Y. Huen, X.-h. Feng, T. Liu, J. Huang, AUNIP/C1orf135 directs DNA double-strand breaks towards the homologous recombination repair pathway. *Nat. Commun.* **8**, 985 (2017).

40. Y. Mu, J. Lou, M. Srivastava, B. Zhao, X.-h. Feng, T. Liu, J. Chen, J. Huang, SLFN11 inhibits checkpoint maintenance and homologous recombination repair. *EMBO Rep.* **17**, 94–109 (2016).